Ligand-Transformation Syntheses and Stereophysical Investigations of 48-Electron Mixed Cp/Cp′ Triangular $MnFe_2$ Clusters Containing $MnFe_2(\mu_2\text{-}CO)_2(\mu_2\text{-}NO)(\mu_3\text{-}NX)$ Cores (Where X = O, OH, OMe, H): Structural-Bonding Consequences Due to Conversions of a Capping Nitrosyl (μ_3-NO) Ligand into Electronically Equivalent $(\mu_3\text{-}NOR)^+$ Ligands (R = H, Me) and into an Imido $(\mu_3\text{-}NH)^+$ Ligand and to the One-Electron Reduction of an Imido-Capped $MnFe_2$ Cluster

Mary E. Barr,[1a,b] Asgeir Bjarnason,[1c] and Lawrence F. Dahl*,[1a]

Department of Chemistry, University of Wisconsin—Madison, Madison, Wisconsin, 53706, and Science Institute, University of Iceland, Dunhaga 3, IS-107 Reykjavik, Iceland

Received January 20, 1993®

Ligand-transformation syntheses of a series of 48-electron mixed Cp/Cp′ triangular heterometallic clusters containing $MnFe_2(\mu_2\text{-}CO)_2(\mu_2\text{-}NO)(\mu_3\text{-}NX)$ cores (where Cp and Cp′ denote $\eta^5\text{-}C_5H_5$ and $\eta^5\text{-}C_5H_4Me$, respectively; X = O, OH, OMe, and H) are presented herein. These compounds were characterized by single-crystal X-ray diffraction, IR, ^1H NMR, laser-desorption FT mass spectrometric, and electrochemical studies; one reduced 49-electron cluster was additionally characterized by EPR measurements. The $(\mu_3\text{-}NH)^+$-containing imido $MnFe_2$ monocations were obtained directly (i.e., with no detectable $(\mu_3\text{-}NOH)^+$-containing intermediates) from their neutral (μ_3-NO)-containing nitrosyl analogues in CH_2Cl_2 either by proton-induced reduction in reactions with $HBF_4{\cdot}OR_2$ (R = Me, Et) (40% yields) or by oxidation-induced reductive deoxygenation in reactions with a variety of oxidants (Ag^+, NO^+, NO_2^+, Br_2, I_2) and presumably adventitious water as the proton source (10–40% yields). The two electrons required for the formal reduction of each (μ_3-NO) ligand into the $(\mu_3\text{-}NH)^+$ ligand are provided by other "sacrificial" clusters (i.e., most likely by metal atoms in the acid reactions and CO/NO ligands in the oxidation reactions). Methylation reactions converted the (μ_3-NO)-containing $MnFe_2$ clusters into corresponding $(\mu_3\text{-}NOMe)^+$-containing monocations (40–50% yields); the $(\mu_3\text{-}NOH)^+$-containing $MnFe_2$ monocation was isolated from the reaction of a (μ_3-NO)-containing cluster with dilute triflic acid formed via the hydrolysis of methyl triflate with adventitious water in the CH_2Cl_2 solvent. All of these 48-electron $MnFe_2$ clusters, which contain the same $MnFe_2(\mu_2\text{-}CO)_2(\mu_2\text{-}NO)(\mu_3\text{-}N)$ fragment exhibit pseudo-C_s-m symmetry with similar electron-pair Fe–Fe (2.44 ± 0.01 Å) and Fe–Mn (2.57 ± 0.01 Å) bonding distances; their core geometries are also not significantly affected by an interchange of Cp and Cp′ ligands. The noncylindrical $(\mu_3\text{-}NOR)^+$ ligands in these clusters were found to possess a particular geometrical orientation relative to the $MnFe_2$ triangle. Observed variations in metal–nitrogen distances to the capping ligands are consistent with the proposed changes in the bonding interactions of the metal atoms with the $(\mu_3\text{-}NOR)^+$ (R = H, Me) and $(\mu_3\text{-}NH)^+$ ligands relative to those with the parent (μ_3-NO) ligand. The marked changes in geometry observed upon reduction of the 48-electron imido-capped $[Cp'MnFe_2Cp'_2(\mu_2\text{-}CO)_2(\mu_2\text{-}NO)(\mu_3\text{-}NH)]^+$ monocation to its 49-electron neutral species correspond to the previously determined geometrical differences between the corresponding members of the closely related 48/49-electron nitrosyl-capped $[Cp'MnFe_2Cp_2(\mu_2\text{-}CO)_2(\mu_2\text{-}NO)(\mu_3\text{-}NO)]^n$ series (n = 0, 1−). The analogous changes in overall core geometries coupled with both 49-electron species displaying similar EPR spectra (with no discernible hyperfine interactions) provide convincing evidence that the unpaired electron in the imido-capped $MnFe_2$ cluster likewise occupies a nondegenerate HOMO (under C_s symmetry) of primarily diiron-antibonding character.

Introduction

Systematic structural-bonding studies in our laboratories of a variety of triangular homonuclear metal cluster systems[2] and in one triangular mixed-metal cluster series[3] have shown that the number of cluster valence electrons (CVEs)[4,5] and the nature of the capping and terminal ligands have a pronounced effect on the geometries of these trimetal clusters. For example, replacement of Cp ligands in the 50/49/48-electron $[Co_3Cp_3(\mu_3\text{-}S)_2]^n$ series (n = 0, 1^+, 2^+)[2e,6–8] with Cp′ ligands (where Cp and Cp′ denote $\eta^5\text{-}C_5H_5$ and $\eta^5\text{-}C_5H_4Me$, respectively) to give the corresponding $[Co_3Cp'_3(\mu_3\text{-}S)_2]^n$ series (n = 0, 1^+, 2^+)[2q]

® Abstract published in *Advance ACS Abstracts,* April 1, 1994.

(1) (a) University of Wisconsin—Madison. (b) Los Alamos National Laboratory, Los Alamos, NM. (c) Science Institute, University of Iceland.

0276-7333/94/2313-1981$04.50/0

results in profoundly different solid-state Co_3S_2 core geometries for the 50-electron neutral parents as well as for their corresponding 49-electron monocations. Thus, while $Co_3Cp_3(\mu_3\text{-}S)_2$ crystallizes with an imposed C_{3h}-3/m site symmetry[2e,9] consistent with its Co_3S_2 core possessing an equilateral or minimally deformed isosceles cobalt triangle, the Co_3S_2 core of $Co_3Cp'_3(\mu_3\text{-}S)_2$ exhibits a markedly distorted C_{2v} geometry with the isosceles cobalt triangle possessing one nonbonding and two electron-pair bonding edges.[2q] Oxidation of $Co_3Cp_3(\mu_3\text{-}S)_2$ to its 49-electron monocation produces an isosceles cobalt triangle with one shorter electron-pair bonding edge and two longer "net one and a half-electron" bonding edges,[2e,10] while extraction of one of the two antibonding electrons from $Co_3Cp'_3(\mu_3\text{-}S)_2$ gives rise to a monocation with an isosceles cobalt triangle containing one longer "net one-electron" bonding edge and two unaltered electron-pair bonding edges.[2q] Furthermore, the analogous mean Co–Co distances for the 50-electron neutral parents in these two series are 0.1 Å longer than those for the 49-electron monocations, which in turn are 0.1 Å longer than those of the 48-electron dications. This linear correlation of the mean metal–metal distance with the number of valence electrons in excess of 48[4,5] is readily attributed to the HOMOs of these 49- and 50-electron clusters possessing considerable trimetal-antibonding orbital character.[2q] Other structural-bonding studies[2i-k] on a series of 48-electron homometallic triangular clusters, $[Co_3(\eta^5\text{-}C_5H_{5-x}Me_x)_3(\mu_3\text{-}X)(\mu_3\text{-}Y)]^n$ (where x = 0, 1, 5; X = CO, NO; Y = NR where R = $SiMe_3$, $C(O)NH_2$, H), revealed that replacement of Cp with Cp′ terminal ligands has minimal effects upon the metal core geometries of these complexes.

The designed synthesis by Kubat-Martin *et al.*[3] of the 48-electron mixed-metal cluster $Cp'MnFe_2Cp_2(\mu_2\text{-}CO)_2(\mu_2\text{-}NO)(\mu_3\text{-}NO)$ and its 49-electron monoanion enabled this research to be expanded into the area of triangular heterometallic systems. The work presented here is an outgrowth of initial attempts[3] to isolate the 47-electron $[Cp'MnFe_2Cp_2(\mu_2\text{-}CO)_2(\mu_2\text{-}NO)(\mu_3\text{-}NO)]^+$ monocation (**7**$^+$); its existence is indicated by cyclic voltammetric measurements which show that the neutral parent (**7**) can undergo a reversible one-electron oxidation as well as a reversible one-electron reduction. Described herein are the preparations and stereophysical studies of five 48-electron $MnFe_2$ clusters, viz., $CpMnFe_2Cp'_2(\mu_2\text{-}CO)_2(\mu_2\text{-}NO)(\mu_3\text{-}NO)$ (**1**), $[CpMnFe_2Cp'_2(\mu_2\text{-}CO)_2(\mu_2\text{-}NO)(\mu_3\text{-}NOMe)]^+$ (**2**), $[Cp'MnFe_2Cp_2(\mu_2\text{-}CO)_2(\mu_2\text{-}NO)(\mu_3\text{-}NOMe)]^+$ (**3**), $[CpMnFe_2Cp'_2(\mu_2\text{-}CO)_2(\mu_2\text{-}NO)(\mu_3\text{-}NOH)]^+$ (**4**), and $[Cp'MnFe_2Cp_2(\mu_2\text{-}CO)_2(\mu_2\text{-}NO)(\mu_3\text{-}NH)]^+$ (**5**), and one reduced 49-electron cluster, $Cp'MnFe_2Cp'_2(\mu_2\text{-}CO)_2(\mu_2\text{-}NO)(\mu_3\text{-}NH)$ (**6**). These trimetal clusters have provided the basis for a structural-bonding analysis of geometrical effects arising from (1) the interchange of Cp and Cp′ ligands, (2) ligand transformations involving conversions of the μ_3-NO ligand to $(\mu_3\text{-}NH)^+$, $(\mu_3\text{-}NOMe)^+$, and $(\mu_3\text{-}NOH)^+$ ligands, and (3) the addition of an unpaired electron to a 48-electron imido-capped $MnFe_3$ cluster. Facile conversion of the $(\mu_3$-NO) ligand in these heterometallic clusters to a $(\mu_3\text{-}NH)^+$ ligand occurs via oxidizing agents as well as by strong protic acids. Such a transformation is of particular interest because it requires N–O bond scission and a formal two-electron reduction, and thus may provide a homogeneous parallel to the activation of nitric oxide on a hydrated heterogeneous metal surface to produce nitrogen–hydrogen species under appropriate reducing conditions.

Of particular relevance to this research is the report by Legzdins *et al.*[11] on the isolation of the 48-electron imido-capped $[Mn_3Cp'_3(\mu_2\text{-}NO)_3(\mu_3\text{-}NH)]^+$ monocation from the reaction of the 48-electron $Mn_3Cp'_3(\mu_2\text{-}NO)_3(\mu_3\text{-}NO)$[12-14] cluster with excess acid. They determined that this conversion occurs via a sequential protonation reaction of the $(\mu_3$-NO) ligand to yield an isolated and structurally characterized $(\mu_3\text{-}NOH)^+$-containing intermediate which then reacts with an additional 2 equiv of acid to produce the $(\mu_3\text{-}NH)^+$-containing monocation (and water). They speculated that the two electrons required for this formal reduction of the $(\mu_3\text{-}NOH)^+$ cluster to the $(\mu_3\text{-}NH)^+$ cluster are most likely provided intermolecularly by the manganese atoms of another "sacrificial" cluster. These proton-induced reductive μ_3-NO ligand-transformation reactions are related to the classic studies by Shriver and co-workers[15] on the proton-induced reduction of the μ_3-CO ligand in the $[Fe_4(CO)_{12}(\mu_3\text{-}CO)]^{2-}$ dianion[16] into methane.[17,18]

Similar ligand-transformation reactions of doubly bridging nitrosyl ligands in triangular metal clusters have been reported. Gladfelter and co-workers[19] found that O-methylation and O-protonation of the μ_2-NO ligand in the 48-electron $[Ru_3(CO)_{10}(\mu_2\text{-}NO)]^-$ monoanion occurs with CF_3SO_3Me and CF_3SO_3H, respectively, resulting in the

(2) (a) Vahrenkamp, H.; Uchtman, V. A.; Dahl, L. F. *J. Am. Chem. Soc.* **1968**, *90*, 3272–3273. (b) Uchtman, V. A.; Dahl, L. F. *J. Am. Chem. Soc.* **1969**, *91*, 3763–3769. (c) Strouse, C. E.; Dahl, L. F. *Discuss. Faraday Soc.* **1969**, No. 47, 93–106. (d) Strouse, C. E.; Dahl, L. F. *J. Am. Chem. Soc.* **1971**, *93*, 6032–6041. (e) Frisch, P. D.; Dahl, L. F. *J. Am. Chem. Soc.* **1972**, *94*, 5082–5084. (f) Byers, L. R.; Uchtman, V. A.; Dahl, L. F. *J. Am. Chem. Soc.* **1981**, *103*, 1942–1951. (g) Maj, J. A.; Rae, A. D.; Dahl, L. F. *J. Am. Chem. Soc.* **1982**, *104*, 3054–3063. (h) Kubat-Martin, K. A.; Rae, A. D.; Dahl, L. F. *Organometallics* **1985**, *4*, 2221–2223. (i) Bedard, R. L.; Rae, A. D.; Dahl, L. F. *J. Am. Chem. Soc.* **1986**, *108*, 5924–5932. (j) Bedard, R. L.; Dahl, L. F. *J. Am. Chem. Soc.* **1986**, *108*, 5933–5942. (k) Bedard, R. L.; Dahl, L. F. *J. Am. Chem. Soc.* **1986**, *108*, 5942–5948. (l) Olson, W. L.; STacy, A. M.; Dahl, L. F. *J. Am. Chem. Soc.* **1986**, *108*, 7646–7656. (m) Olson, W. L.; Dahl, L. F. *J. Am. Chem. Soc.* **1986**, *108*, 7657–7663. (n) North, T. E.; Thoden, J. B.; Spencer, B.; Bjarnason, A.; Dahl, L. F. *Organometallics* **1992**, *11*, 4326–4337. (o) North, T. E.; Thoden, J. B.; Spencer, B.; Dahl, L. F. *Organometallics* **1992**, *12*, 1294–1313. (p) Ziebarth, M. S.; Dahl, L. F. *J. Am. Chem. Soc.* **1990**, *112*, 2411–2418. (q) Pulliam, C. R.; Thoden, J. B.; Stacy, A. M.; Spencer, B.; Englert, M. H.; Dahl, L. F. *J. Am. Chem. Soc.* **1991**, *113*, 7398–7410.

(3) Kubat-Martin, K. A.; Spencer, B.; Dahl, L. F. *Organometallics* **1987**, *6*, 2580–2587.

(4) The Lauher electron-counting procedure[5] is utilized herein to bookkeep the observed number of cluster valence electrons (CVEs). Any valence electrons in excess of the 48 CVEs normally found in a completely bonding triangular metal cluster would occupy the higher-lying frontier MOs that, in general, are trimetal-antibonding.

(5) Lauher, J. W. *J. Am. Chem. Soc.* **1978**, *100*, 5305–5315.

(6) (a) Otsuka, S.; Nakamura, A.; Yoshida, T. *Inorg. Chem.* **1968**, *7*, 261–265. (b) Otsuka, S.; Nakamura, A.; Yoshida, T. *Justus Liebigs Ann. Chem.* **1968**, *719*, 54–60.

(7) Sorai, M.; Kosaki, A.; Suga, H.; Seki, S.; Yoshida, T.; Otsuka, S. *Bull. Chem. Soc. Jpn.* **1971**, *44*, 2364–2371.

(8) Madach, T.; Vahrenkamp, H. *Chem. Ber.* **1981**, *114*, 505–512.

(9) Kamijo, N.; Watanabe, T. *Acta Crystallogr.* **1979**, *B35*, 2537–2542.

(10) Teo, B.-K. Ph.D. Thesis, University of Wisconsin—Madison, Madison, WI, 1973.

(11) Legzdins, P.; Nurse, C. R.; Retig, S. J. *J. Am. Chem. Soc.* **1983**, *105*, 3727–3728.

(12) Kolthammer, B. W. S.; Legzdins, P. *J. Chem. Soc., Dalton Trans.* **1978**, 31–35.

(13) This cluster is an analogue of the structurally known prototype, $Mn_3Cp_3(\mu_2\text{-}NO)_3(\mu_3\text{-}NO)$.[14]

(14) Elder, R. C. *Inorg. Chem.* **1974**, *13*, 1037–1042.

(15) (a) Whitmire, K. H.; Shriver, D. F. *J. Am. Chem. Soc.* **1980**, *102*, 1456–1457. (b) Whitmire, K. H.; Shriver, D. F.; Holt, E. M. *J. Am. Chem. Soc., Chem. Commun.* **1980**, 780–781. (c) Holt, E. M.; Whitmire, K. H.; Shriver, D. F. *J. Organomet. Chem.* **1981**, *213*, 125–137. (d) Whitmire, K. H.; Shriver, D. F. *J. Am. Chem. Soc.* **1981**, *103*, 6754–6755. (e) Drezdzon, M. A.; Whitmire, K. H.; Bhattacharyya, A. A.; Hsu, W.-L.; Nagel, C. C.; Shore, S. G.; Shriver, D. F. *J. Am. Chem. Soc.* **1982**, *104*, 5630–5633. (f) Drezdzon, M. A.; Shriver, D. F. *J. Mol. Catal.* **1983**, *21*, 81–93. (g) Horwitz, C. P.; Shriver, D. F. *Adv. Organomet. Chem.* **1984**, *23*, 219–303 and references cited therein.

(16) Doedens, R. J.; Dahl, L. F. *J. Am. Chem. Soc.* **1966**, *88*, 4847–4855.

formation of $(\mu_3\text{-NOMe})^+$ and $(\mu_3\text{-NOH})^+$ ligands in the neutral $Ru_3(CO)_9(\mu_3\text{-CO})(\mu_3\text{-NOR})$ clusters (R = Me, H). Addition of the $[CF_3SO_3]^-$ anion to the $(\mu_3\text{-NOH})^+$-containing cluster gave rise to $Ru_3(CO)_{10}(\mu_2\text{-NO})(\mu_2\text{-H})$ via an O–H to M–H tautomerization. Stone and coworkers[20] also observed a μ_2-NO to $(\mu_3\text{-NOH})^+$ conversion upon protonation of the 48-electron $[(CO)_6Fe_2WCp(\mu_2\text{-CO})(\mu_2\text{-NO})(\mu_3\text{-CR})]^-$ monoanion (R = C_6H_4Me-4) with $HBF_4\cdot OEt_2$, which yielded $(OC)_6Fe_2WCp(\mu_2\text{-CO})(\mu_2\text{-CR})(\mu_3\text{-NOH})$.

Experimental Section

Preparation and Physical/Electrochemical Properties of $CpMnFe_2Cp'_2(\mu_2\text{-CO})_2(\mu_2\text{-NO})(\mu_3\text{-NO})$ (1), $[CpMnFe_2Cp'_2(\mu_2\text{-CO})_2(\mu_2\text{-NO})(\mu_3\text{-NOMe})]^+$ (2), $[Cp'MnFe_2Cp_2(\mu_2\text{-CO})_2(\mu_2\text{-NO})(\mu_3\text{-NOMe})]^+$ (3), $[CpMnFe_2Cp'_2(\mu_2\text{-CO})_2(\mu_2\text{-NO})(\mu_3\text{-NOH})]^+$ (4), $[Cp'MnFe_2Cp_2(\mu_2\text{-CO})_2(\mu_2\text{-NO})(\mu_3\text{-NH})]^+$ (5), and $Cp'MnFe_2Cp'_2(\mu_2\text{-CO})_2(\mu_2\text{-NO})(\mu_3\text{-NH})$ (6). (a) General Procedures. All reactions, sample transfers, and manipulations were performed with oven-dried standard Schlenk-type glassware under nitrogen, either on a vacuum line or in a Vacuum Atmospheres glovebox. The following solvents were dried and distilled prior to use: CH_3CN ($CaSO_4$), THF (potassium/benzophenone), toluene (sodium), CH_2Cl_2 (CaH_2), and hexane (Skelly B cut, CaH_2). $MnCp(CO)_3$ (Strem), CF_3SO_3Me (methyl triflate), $HBF_4\cdot O(CH_3)_2$, [PPN][BH_4], Proton Sponge (Aldrich), Br_2, and other common reagents were purchased and used without further purification. $Fe_2Cp_2(\mu_2\text{-NO})_2$ and $Fe_2Cp'_2(\mu_2\text{-NO})_2$ were prepared from described procedures.[21] $CpMnFe_2Cp'_2(\mu_2\text{-CO})_2(\mu_2\text{-NO})(\mu_3\text{-NO})$ (1), $Cp'MnFe_2Cp_2(\mu_2\text{-CO})_2(\mu_2\text{-NO})(\mu_3\text{-NO})$ (7), and $Cp'MnFe_2Cp'_2(\mu_2\text{-CO})_2(\mu_2\text{-NO})(\mu_3\text{-NO})$ were synthesized using the procedure published by Kubat-Martin *et al.*[3]

Solution infrared spectra were recorded on a Beckman 4240 spectrophotometer. ^1H NMR spectra were obtained with Bruker WP-270 and WP-200 spectrometers. Electrochemical data were collected on a BAS-100 electrochemical analyzer with the cell enclosed in a nitrogen-filled Vacuum Atmospheres glovebox. Electrochemical solutions consisted of ca. 7 mL of solvent containing approximately 10^{-3} M compound and 0.1 M [NBu_4][PF_6] electrolyte. The working electrode was a platinum disk, the auxiliary electrode a platinum coil, and the reference electrode a Vycor-tipped aqueous SCE separated from the test solution by a Vycor-tipped salt bridge containing 0.1 M [NBu_4][PF_6] in MeCN. An *iR* compensation for solution resistance[22] was made prior to current–voltage measurements.

Mass spectra were obtained by one of us (A.B.) with an EXTREL FTMS-2000 Fourier transform (FT) mass spectrometer equipped with a 3.0-T superconducting magnet, an EXTREL laser desorption (LD) interface, and a Tachisto 215G resonator. Additional details of the LD-FTMS instrument and procedures for sample preparation and data collection are available elsewhere.[23]

(b) $CpMnFe_2Cp'_2(\mu_2\text{-CO})_2(\mu_2\text{-NO})(\mu_3\text{-NO})$ (1). 1 was synthesized via the procedure developed by Kubat-Martin *et al.*[3] A typical reaction used $MnCp(CO)_3$ (0.52 g; 2.55 mmol) and $Fe_2Cp'_2(\mu_2\text{-NO})_2$ (0.30 g; 0.91 mmol) to produce olive green 1 (0.37 g; 0.73 mmol) in approximately 80% yield.

Solution infrared spectrum (CH_2Cl_2): 1830 (s, μ_2-CO), 1790 (s, μ_2-CO), 1515 (m, μ_2-NO), and 1320 (m, μ_3-NO) cm^{-1}. Solid-state IR spectrum (KBr): 1820 (s, μ_2-CO), 1775 (s, μ_2-CO), 1510 (m, μ_2-NO), and 1315 (m, μ_3-NO) cm^{-1}. ^1H NMR spectrum (200 MHz; CD_2Cl_2; 310 K): δ 4.92 (5H, Cp), 4.44 (2H, Cp'), 4.36 (4H, Cp'), 4.28 (2H, Cp'), and 1.72 (6H, Me) ppm.

The most abundant fragment-ion peak in a positive-ion LD/FT mass spectrum of 1 is the parent-ion peak, $[M]^+$, at m/z 506 (100%). Assigned lower-mass fragment-ion peaks are detected at m/z 450 ($[M - 2CO]^+$; 70%), 420 ($[M - 2CO - NO]^+$; 12%), and 214 ($[Cp'_2Fe]^+$; 46%). Assigned higher-mass fragment-ion peaks are detected at m/z 626 ($[M + MnCp]^+$; 50%), 780 ($[CpMnFe_4Cp'_4(NO)_4]^+$; 44%), and 956 ($[Cp_2Mn_2Fe_4Cp'_4(CO)_2(NO)_4]^+$; 11%). These higher-mass ion fragments were not observed in an EI (15 eV) mass spectrum[3] of the analogous $Cp'MnFe_2Cp_2(\mu_2\text{-CO})_2(\mu_2\text{-NO})(\mu_3\text{-NO})$ cluster (7). A cyclic voltammogram of 1 (50 mV/s; CH_2Cl_2) exhibits two reversible electrochemical processes with $E_{1/2(ox)}$ = 0.59 V (ΔE_p = 63 mV) and $E_{1/2(red)}$ = −1.12 V (ΔE_p = 77 mV). These oxidation and reduction potentials are virtually identical to those reported for 7 (+0.60 and −1.08 V).[3]

Another derivative of 1, $Cp'MnFe_2Cp'_2(\mu_2\text{-CO})_2(\mu_2\text{-NO})(\mu_3\text{-NO})$, was obtained via a procedure similar to that used above. This $Cp'MnFe_2Cp'_2$ cluster, used in the synthesis of 6, was generated from a reaction of $Fe_2Cp'_2(\mu_2\text{-NO})_2$ (0.28 g; 0.85 mmol) with an excess of $MnCp'(CO)_3$ in 82% yield (0.36 g; 0.70 mmol). Solution infrared spectrum (THF): 1830 (s, μ_2-CO), 1795 (s, μ_2-CO), 1518 (m, μ_2-NO), and 1321 (s, μ_3-NO) cm^{-1}. ^1H NMR spectrum (270 MHz; $CDCl_3$; 310 K): two equivalent Cp' ligands at δ 4.72 (4H, Cp'), 4.39 (4H, Cp'), and 1.74 (6H, Me) ppm and one nonequivalent Cp' ligand at δ 4.32 (2H, Cp'), 4.24 (2H, Cp'), and 1.94 (3H, Me) ppm. A cyclic voltammogram (200 mV/s; CH_2Cl_2) exhibits one reversible oxidation and one reversible reduction at $E_{1/2(ox)}$ = 0.53 V (ΔE_p = 90 mV) and $E_{1/2(red)}$ = −1.20 V (ΔE_p = 120 mV).

(c) $[CpMnFe_2Cp'_2(\mu_2\text{-CO})_2(\mu_2\text{-NO})(\mu_3\text{-NOMe})]^+$ (2) and $[Cp'MnFe_2Cp_2(\mu_2\text{-CO})_2(\mu_2\text{-NO})(\mu_3\text{-NOMe})]^+$ (3). 2 and 3 were prepared and isolated as their $[CF_3SO_3]^-$ salts from similar reactions. The procedure given is for the synthesis of 2.

In a typical reaction, 1 (0.33 g; 0.65 mmol) was loaded into a 50 mL flask and dissolved in ca. 25 mL of CH_2Cl_2 to give a green solution. This flask and another flask containing methyl triflate (CF_3SO_3Me) were attached to a high-vacuum line equipped with a mercury manometer; after the solutions were frozen in liquid nitrogen, the entire system was evacuated. Approximately 3 equiv of methyl triflate (as 50 cm^3 of gas measured via a change in line pressure) was added to the reaction vessel in four successive transfers. The resulting reddish solution was stirred under N_2 for 1 h. The solvent was then stripped from the products under vacuum. Extraction with toluene (3×) removed the unreacted starting materials. The remaining red solid was extracted first with CH_2Cl_2 and then with THF. Both extracts contained only 2, and the approximate yield of 2 was 40–50% (based on recovered starting material (1)).

Solid-state IR spectrum (KBr) of 2 as the $[CF_3SO_3]^-$ salt: 3080 (w, C–H), 1900 (s, μ_2-CO), 1870 (m, μ_2-CO), 1830 (s, μ_2-CO), and 1545 (m, μ_2-NO) cm^{-1}. Several lower frequency bands were observed, but none may be unambiguously assigned to the N–OMe stretching mode. ^1H NMR spectrum (200 MHz; acetone-d_6; 310 K) of 2: δ 5.55 (5H, Cp), 5.46 (3H, μ_3-NOMe), 5.27 (2H, Cp'), 5.13 (4H, Cp'), 5.05 (2H, Cp'), and 1.71 (6H, Me) ppm.

(17) This sequential conversion occurs via formation of the intermediate $[Fe_4(CO)_{12}(\mu_2\text{-H})(\eta^2,\mu_4\text{-CO})]^-$ monoanion, which possesses an open-edge tetrahedral (butterfly) iron fragment coordinated to the four-electron-donating η^2-CO ligand.[18] Further protonation produces an (η^2-COH)-containing cluster whose reduction to form a (η^2-CH)-containing intermediate, $Fe_4(CO)_{12}(\mu_2\text{-H})(\eta^2\text{-CH})$, and water requires 2 equiv of protons and two electrons (which are apparently supplied by sacrificial oxidation of an iron species).[15]

(18) Manassero, M.; Sansoni, M.; Longoni, G. *J. Chem. Soc., Chem. Commun.* **1976**, 919–920.

(19) (a) Stevens, R. E.; Gladfelter, W. L. *J. Am. Chem. Soc.* **1982**, *104*, 6454–6457. (b) Stevens, R. E.; Guettler, R. D.; Galdfelter, W. L. *Inorg. Chem.* **1990**, *29*, 451–456.

(20) Delgado, E.; Jeffery, J. C.; Simmons, N. D.; Stone, F. G. A. *J. Chem. Soc., Dalton Trans.* **1986**, 869–873.

(21) (a) Brunner, H. J. *Organomet. Chem.* **1968**, *14*, 173–178. (b) Kubat-Martin, K. A.; Barr, M. E.; Spencer, B.; Dahl, L. F. *Organometallics* **1987**, *6*, 2570–2579.

(22) He, P.; Avery, J. P.; Faulkner, L. R. *Anal. Chem.* **1982**, *54*, 1313A–1326A.

(23) (a) Bjarnason, A.; DesEnfants, R. E., II; Barr, M. E.; Dahl, L. F. *Organometallics* **1990**, *9*, 657–661. (b) Bjarnason, A. *Rapid Commun. Mass Spectrom.* **1989**, *3*, 373–376.

The $[Cp'MnFe_2Cp_2(\mu_2\text{-}CO)_2(\mu_2\text{-}NO)(\mu_3\text{-}NOMe)]^+$ monocation (**3**) was synthesized from **7** (0.34 g). The reaction procedure, workup, and estimated yield for **3** are analogous to that given above for **2**. Infrared spectrum (KBr) of **3** as the triflate salt: 3100 (w), 1880 (s), 1845 (m), 1835 (s), and 1560 (m) cm^{-1}. Interpretation of the proton NMR spectrum (200 MHz; acetone-d_6; 310 K) is complicated by accidental chemical-shift equivalency of the methyl protons of the μ_3-NOMe ligand with one set of the Cp′ ring AA′BB′ protons. A signal at δ 5.50 (5H) ppm is assigned to these two groups. Other resonances are δ 5.45 (2H, Cp′), 5.31 (10H, Cp), and 1.92 (3H, Me) ppm.

Cyclic voltammograms of **2** and **3** reveal that neither compound undergoes any reversible oxidation or reduction processes. A CV of **2** (200 mV/s; CH_2Cl_2) exhibits two reduction waves at E_p = −0.43 and −1.22 V and one oxidation wave at E_p = 1.25 V. Under the same conditions, **3** exhibits two reduction waves at E_p = −0.55 and −1.18 V and an oxidation wave at E_p = 1.31 V.

(d) $[CpMnFe_2Cp'_2(\mu_2\text{-}CO)_2(\mu_2\text{-}NO)(\mu_3\text{-}NOH)]^+$ (4). **4** was an unintentional product in an attempt to synthesize the $[CpMnFe_2Cp'_2(\mu_2\text{-}CO)_2(\mu_2\text{-}NO)(\mu_3\text{-}NMe)]^+$ monocation from a reaction of excess methyl triflate with **1**. Presumably, the CH_2Cl_2 solvent used in this reaction was not sufficiently dry, or the methyl triflate had hydrolyzed since its previous use.

In this reaction, $CpMnFe_2Cp'_2(\mu_2\text{-}CO)_2(\mu_2\text{-}NO)(\mu_3\text{-}NO)$ (**1**) (0.20 g; 0.40 mmol) was dissolved in 25 mL of CH_2Cl_2 in a 100-mL flask. A solution containing a large excess of CF_3SO_3Me (500 μL) in CH_2Cl_2 was added slowly (30 min) to the flask with constant swirling. The solution changed from green to red/brown during the addition, after which it was allowed to stir for an additional 1 h. The solvent was then removed under vacuum, and the resultant solid extracted with toluene to remove unreacted starting materials. The majority of **1** was recovered unchanged. The red solid (**4**) (estimated yield 20–30%) was extracted with CH_2Cl_2.

Solid-state infrared spectrum (KBr) of **4**: 3340 (w, broad, NO–H), 1865 and 1830 (s, μ_2-CO), and 1545 cm^{-1} (m, μ_2-NO). ^1H NMR spectrum (200 MHz; CD_2Cl_2): δ 5.31 (5H, Cp), 5.08 (1H, t, $^2J_{N-H}$ 20 Hz, μ_3-NOH), 4.96 (2H, Cp′), 4.85 (4H, Cp′), 4.75 (2H, Cp′), and 1.72 (6H, Me) ppm. A cyclic voltammogram (100 mV/s; CH_2Cl_2) of **4** displays a reversible oxidation at $E_{1/2(ox)}$ = 0.55 V (ΔE_p = 61 mV) and two closely spaced irreversible reduction waves at E_p = −0.38 and −0.42 V.

(e) $[Cp'MnFe_2Cp_2(\mu_2\text{-}CO)_2(\mu_2\text{-}NO)(\mu_3\text{-}NH)]^+$ (5). **5** may be formed either by protonation or by chemical oxidation of the neutral parent **7**. It has been isolated as the only cationic species in chemical oxidation reactions with Ag^+, NO^+, NO_2^+, Br_2, or I_2 and in protonation reactions with $HBF_4{\cdot}OR_2$ (R = Me or Et). It was first isolated as the $[PF_6]^-$ salt (10% yield) in an attempted oxidation of **7** with $AgPF_6$.[3,24] A more rational, higher-yield protonation route is given below along with an alternative oxidative method.

Method 1. In a typical reaction, $Cp'MnFe_2Cp_2(\mu_2\text{-}CO)_2(\mu_2\text{-}NO)(\mu_3\text{-}NO)$ (**7**) (0.50 g; 1.0 mmol) was dissolved in ca. 30 mL of CH_2Cl_2. A solution of $HBF_4{\cdot}OMe_2$ (270 μL; 2.0 mmol) in CH_2Cl_2 was added dropwise to the reaction vessel while the solution was stirred vigorously. The progress of the reaction was monitored via periodic IR spectra; the bridging carbonyl bands shifted from 1835 and 1790 cm^{-1} in the neutral starting material to 1885 and 1850 cm^{-1} in the cationic product as the reaction progressed. After 1.5 equiv of $HBF_4{\cdot}OMe_2$ had been added, IR spectra indicated that the starting material had been completely consumed. The solvent was then removed under a nitrogen purge, and the reddish residue was extracted (3×) with toluene to remove unreacted starting materials. Red **5** (0.23 g; 40% yield) was extracted with CH_2Cl_2. Approximately half of the total material remained as an insoluble reddish powder. The amount of this insoluble residue relative to the amount of isolated **5** increased dramatically in reactions where 2 and 3 equiv of $HBF_4{\cdot}OMe_2$ were used.

The $[BF_4]^-$ salt of **5** was dissolved in THF, metathesized with $[Na][BPh_4]$, and then extracted with CH_2Cl_2 in order to isolate the tetraphenylborate salt of **5** for X-ray crystallographic and mass spectral analyses.

Method 2. In this reaction, a solution of **7** (0.33 g; 0.67 mmol) in 30 mL of CH_2Cl_2 was titrated with a dilute solution of Br_2 (250 μL) in CH_2Cl_2 (70 mL). The progress of the reaction was monitored via IR spectra as outlined above. The reaction was halted after 2 equiv of Br_2 had been added. At this point the IR spectra indicated that approximately half of the neutral starting material had been converted to a cationic species. The solvent was then removed under a nitrogen purge. The resultant reddish solid was washed with toluene to recover unreacted **7**. The remainder of the ruby-colored solid was dissolved in THF. The estimated yield of **5**, isolated as the $[FeBr_4]^-$ salt, was 40% (based on recovered **7**).

Solid-state IR spectrum (KBr) of **5**: 3340 (w, N–H), 1880 and 1835 (s, μ_2-CO), and 1555 (m, μ_2-NO) cm^{-1}. ^1H NMR spectrum (270 MHz; acetone-d_6; 310 K): δ 5.22 (2H, Cp′), 5.13 (2H, Cp′), 4.99 (10H, Cp), and 2.04 (3H, Me) ppm. Another ^1H NMR spectrum (200 MHz; CD_2Cl_2) was later run in which the μ_3-NH proton resonance was located at δ 24.92 ppm (t, J_{N-H} 57 Hz).

Positive-ion LD/FT mass spectra of **5** with $[BF_4]^-$ and $[BPh_4]^-$ counterions yield similar fragment-ion peaks: the parent-ion peak $[M]^+$ at m/z 477, $[M-2CO]^+$ at m/z 421, $[M-2CO-H]^+$ at m/z 420, $[Cp'_2Fe]^+$ at m/z 214, $[Cp'FeCp]^+$ at m/z 200, and $[Cp_2Fe]^+$ at m/z 186. A cyclic voltammogram (200 mV/s; THF) reveals that **5** undergoes two reversible reductions at $E_{1/2}$ = −0.39 and −1.13 V (ΔE_p = 68 and 101 mV, respectively).

(f) $Cp'MnFe_2Cp'_2(\mu_2\text{-}CO)_2(\mu_2\text{-}NO)(\mu_3\text{-}NH)$ (6). $[Cp'MnFe_2Cp'_2(\mu_2\text{-}CO)_2(\mu_2\text{-}NO)(\mu_3\text{-}NH)][PF_6]$ was prepared from the reaction of $Cp'MnFe_2Cp'_2(\mu_2\text{-}CO)_2(\mu_2\text{-}NO)(\mu_3\text{-}NO)$ with $AgPF_6$ as described by Kubat-Martin[3,24] and characterized via IR analysis. A CV (200 mV/s; THF) of this monocation displays electrochemical behavior analogous to that of **5** with two reversible reductions at $E_{1/2}$ = −0.48 and −1.22 V (ΔE_p = 81 and 111 mV, respectively). The $[BH_4]^-$ anion was chosen as a reductant which would be sufficiently strong to produce the first reduction to the neutral system without causing further reduction to the monoanion.

In this reaction, $[PPN][BH_4]$ (0.12 g; 0.2 mmol) in 30 mL of CH_2Cl_2 was added to $[Cp'MnFe_2Cp'_2(\mu_2\text{-}CO)_2(\mu_2\text{-}NO)(\mu_3\text{-}NH)][PF_6]$ (0.05 g; 0.1 mmol) in a 50-mL flask, and the mixture was stirred under a nitrogen atmosphere overnight. The solvent was then removed under a N_2 purge, and the resultant greenish solid was extracted (2×) with toluene. The combined extracts contained only **6** (approximately 70–80% yield).

Solid-state IR spectrum (KBr) of **6**: 3330 (w, μ_3-NH), 1870 and 1825 (s, μ_2-CO), and 1535 (m, μ_2-NO) cm^{-1}. A solution EPR spectrum of **6** displays a single signal with no apparent hyperfine interactions at g = 2.03 (line width = 37 G at 300 K).

(g) Attempted Deprotonation of $[Cp'MnFe_2Cp_2(\mu_2\text{-}CO)_2(\mu_2\text{-}NO)(\mu_3\text{-}NH)]^+$ (5). Attempts were made to chemically deprotonate the $(\mu_3\text{-}NH)^+$ ligand of **5** to a μ_3-N ligand via reagents of varying basicity, viz., anhydrous NEt_3, Proton Sponge, KOH/acetone (0.05 M and 0.01 M), and CH_3Li. In each reaction, a THF solution (or acetone solution for KOH) containing 2–3 equiv of the base was titrated into a THF solution of **5**. The progress of the reaction was monitored via infrared spectroscopy; the absorption bands of the μ_2-CO and μ_2-NO ligands were anticipated to shift to lower frequencies upon deprotonation of the monocation **5** to its neutrally charged conjugate base.

Titration with the two solutions of KOH/acetone resulted in immediate decomposition of **5**. A similar titration with the weaker amine base NEt_3 produced no apparent reaction. Reactions of **5** with both Proton Sponge and CH_3Li resulted in the formation of a neutrally charged species with the anticipated infrared spectral shift; however, upon extraction of this product in toluene and subsequent crystallization of the extract from a THF/hexane layered diffusion, it was discovered that the crystallized neutral product was $Cp'MnFe_2Cp_2(\mu_2\text{-}CO)_2(\mu_2\text{-}NO)(\mu_3\text{-}NO)$ (**7**). The μ_3-NO absorption band was not evident in the original reaction

(24) Kubat-Martin, K. A. Ph.D. Thesis, University of Wisconsin—Madison, Maidson, WI, 1986.

Table 1. Crystal, Data-Collection, and Structural Refinement Parameters for $CpMnFe_2Cp'_2(\mu_2\text{-}CO)_2(\mu_2\text{-}NO)(\mu_3\text{-}NO)$ (1), $[CpMnFe_2Cp'_2(\mu_2\text{-}CO)_2(\mu_2\text{-}NO)(\mu_3\text{-}NOMe)]^+[CF_3SO_3]^-\cdot{}^1/_2CH_2Cl_2$ ([2][CF_3SO_3]$\cdot{}^1/_2CH_2Cl_2$), $[Cp'MnFe_2Cp_2(\mu_2\text{-}CO)_2(\mu_2\text{-}NO)(\mu_3\text{-}NOMe)]^+[CF_3SO_3]^-$ ([3][CF_3SO_3]), $[CpMnFe_2Cp'_2(\mu_2\text{-}CO)_2(\mu_2\text{-}NO)(\mu_3\text{-}NOH)]^+[CF_3SO_3]^-$ ([4][CF_3SO_3]), $[Cp'MnFe_2Cp_2(\mu_2\text{-}CO)_2(\mu_2\text{-}NO)(\mu_3\text{-}NH)]^+$ (5) (as [5][BPh_4]$\cdot{}^1/_2$THF and [5][$FeBr_4$]), and $Cp'MnFe_2Cp'_2(\mu\text{-}CO)_2(\mu_2\text{-}NO)(\mu_3\text{-}NH)$ (6)

	1	2	3	4	[5][BPh_4]	[5][$FeBr_4$]	6
fw	506.0	712.6	656.1	656.1	832.3	852.5	505.0
cryst syst	monoclinic	monoclinic	triclinic	orthorhombic	monoclinic	monoclinic	triclinic
cell const temp, °C	25	−100	−100	−100	25 (rt)[a]	−100	−100
a, Å	9.427(2)	18.629(3)	9.094(2)	10.267(3)	12.892(4)	9.052(2)	6.151(1)
b, Å	12.854(4)	19.423(4)	10.257(2)	17.895(6)	11.046(4)	18.643(9)	10.457(2)
c, Å	15.548(4)	14.728(3)	12.923(3)	24.667(8)	26.830(2)	14.800(6)	15.306(3)
α, deg	90	90	93.06(2)	90	90	90	87.45(2)
β, deg	95.37(2)	102.34(2)	107.69(1)	90	98.36(2)	95.30(3)	83.87(2)
γ, deg	90	90	92.89(1)	90	90	90	76.24(2)
V, Å^3	1875.8(8)	5206(2)	1144.0(4)	4523(2)	3780(2)	2487(2)	950.6(3)
space group	$P2_1/c$	$C2/c$	$P\bar{1}$	$Pbcn$	$P2_1/n$	$P2_1/c$	$P\bar{1}$
z	4	8	2	8	4	4	2
d_{calcd}, g/cm^3	1.79	1.82	1.90	1.92	1.46	2.28	1.76
μ, mm^{-1}	2.22	1.83	1.88	1.98	1.13	8.66	2.18
data col temp, °C	25	−100	−100	−100	25 (rt)	−100	−100
radiation	Mo Kα	Mo Kα	Mo Kα	Mo Kα	Mo Kα	Mo Kα	Mo Kα
scan mode	Wyckoff	ω	Wyckoff	Wyckoff	Wyckoff	$\theta/2\theta$	$\theta/2\theta$
scan speed, deg/min	3–16	3–29	3–16	3–16	2.4–12	4–29	3–29
scan range, deg	0.4	1.4	0.4	0.4	0.6	2.0	2.0
bkg offset, deg	1.5		0.9	0.6	0.7		
2θ limits, deg	6–55	3–47	3–50	5–55	3–45	3–47	3–45
no. of data collctd	4454	4123	4720	4790	4750	4098	2681
cutoff for obsd data	$F > 3\sigma(F)$	$F > 3\sigma(F)$	$F > 3\sigma(F)$	$F > 3\sigma(F)$	$F > 3\sigma(F)$	$F > 3\sigma(F)$	$F > 3\sigma(F)$
no. of ind obsd data	2991	2702	3639	3618	3055	2230	1949
data/param	11.8/1	7.7/1	11.2/1	11.1/1	6.9/1	8.0/1	7.7/1
wght (fixed)	0.0016	0.0009	0.0009	0.0008	0.0009	0.0019	0.0016
goodness-of-fit, GOF	1.27	1.60	2.46	1.27	1.54	1.16	1.36
$R_1(F)$, $R_2(F)$, %	5.41, 6.89	6.25, 7.23	5.15, 8.40	4.82, 5.51	6.39, 7.37	6.08, 7.11	5.02, 7.04

[a] rt = room temperature.

mixture, so it is presumed that the formation of the μ_3-NO species (7) occurred during workup or crystallization. Later attempts to crystallize the reaction products in the presence of Proton Sponge or CH_3Li were not successful.

(h) Attempted N–O Cleavage of the μ_3-NO Ligand in $CpMnFe_2Cp'_2(\mu_2\text{-}CO)_2(\mu_2\text{-}NO)(\mu_3\text{-}NO)$ (1) and $Cp'MnFe_2Cp_2(\mu_2\text{-}CO)_2(\mu_2\text{-}NO)(\mu_3\text{-}NO)$ (7). The facility with which the N–O bond of the μ_3-NO ligand in 1 and 7 is cleaved with protic and oxidizing reagents to produce the $(\mu_3\text{-}NH)^+$ ligand suggests that N–O cleavage under other conditions might yield the desired μ_3-N ligand. Hence, the reagents CO, H_2, PPh_3, and B_2S_3 were selected as potential oxyphilic reagents.

In a typical reaction, 0.1 g of 1 or 7 was dissolved in ca. 30 mL of THF. In reactions with CO(g) or H_2(g) the solutions were stirred under 20 psi of each gas for several hours at room temperature and then brought to reflux for an additional 2 h. Chromatography of the products revealed small amounts of the iron carbonyl and iron nitrosyl dimers along with the original triangular $MnFe_2$ cluster. In reactions with PPh_3 or B_2S_3, equimolar amounts of each reagent were combined with 1 or 7 in ca. 30 mL of THF; the resulting solution (or slurry for B_2S_3) was allowed to stir at room temperature overnight and then at reflux temperature for several additional hours. Subsequent chromatographic workup of the products revealed that no reaction occurred with either PPh_3 or B_2S_3.

X-ray Crystallographic Determinations of $CpMnFe_2Cp'_2(\mu_2\text{-}CO)_2(\mu_2\text{-}NO)(\mu_3\text{-}NO)$ (1), $[CpMnFe_2Cp'_2(\mu_2\text{-}CO)_2(\mu_2\text{-}NO)(\mu_3\text{-}NOMe)]^+$ (2), $[Cp'MnFe_2Cp_2(\mu_2\text{-}CO)_2(\mu_2\text{-}NO)(\mu_3\text{-}NOMe)]^+$ (3), $[CpMnFe_2Cp'_2(\mu_2\text{-}CO)_2(\mu_2\text{-}NO)(\mu_3\text{-}NOH)]^+$ (4), $[Cp'MnFe_2Cp_2(\mu_2\text{-}CO)_2(\mu_2\text{-}NO)(\mu_3\text{-}NH)]^+$ (5), and $Cp'MnFe_2Cp'_2(\mu_2\text{-}CO)_2(\mu_2\text{-}NO)(\mu_3\text{-}NH)$ (6). Crystals of 1 and [5][BPh_4]$\cdot{}^1/_2$THF were obtained by a layered diffusion of hexane into a saturated THF solution of each compound. Crystals of [2][CF_3SO_3]$\cdot{}^1/_2CH_2Cl_2$, [3][CF_3SO_3], [4][CF_3SO_3], and [5][$FeBr_4$] were grown by a layered diffusion of hexane into a saturated CH_2Cl_2 solution of the compound with a thin layer of toluene inserted between the two solvents (CH_2Cl_2/toluene/hexane) to slow the diffusion process. Intensity data for each compound were collected with graphite-monochromated Mo Kα radiation on a Siemens P3/F diffractometer equipped with a liquid-nitrogen cooling apparatus. Axial photographs were taken to confirm lattice lengths and cell symmetry for all crystals. The SHELXTL Plus 4.11 package[25] was used to apply absorption corrections (analytical for [2][CF_3SO_3]$\cdot{}^1/_2CH_2Cl_2$ and ψ-scans for the other compounds) as well to solve and refine each crystal structure. Heavy-atom positions were determined by direct methods, and the other non-hydrogen atoms were located from difference Fourier syntheses coupled with least-squares refinements. Atomic scattering factors for neutral atoms were used together with anomalous dispersion corrections for all non-hydrogen atoms. Hydrogen atoms for the Me, Cp, Cp′, and/or Ph ligands of 1–6 were inserted at idealized positions with assigned isotropic thermal parameters and were included as fixed contributions in the final stages of anisotropic least-squares refinement. Crystal data, data-collection parameters, and least-squares refinement parameters for 1–6 are presented in Table 1.

Tables of atomic coordinates with equivalent isotropic thermal parameters, tables of anisotropic parameters for the non-hydrogen atoms, and tables of selected bond lengths and angles for compounds 1–6 are included as supplementary material.

Results

Structural Features of $CpMnFe_2Cp'_2(\mu_2\text{-}CO)_2(\mu_2\text{-}NO)(\mu_3\text{-}NO)$ (1) and a Geometrical-Bonding Comparison with $Cp'MnFe_2Cp_2(\mu_2\text{-}CO)_2(\mu_2\text{-}NO)(\mu_3\text{-}NO)$ (7). The monoclinic unit cell ($P2_1/n$) of 1 contains four crystallographically related discrete molecules which pack with no unusual intermolecular contacts. Although the independent molecule of 1 has no crystallographically imposed symmetry, the $MnFe_2(\mu_2\text{-}CO)_2(\mu_2\text{-}NO)(\mu_3\text{-}NO)$ core closely conforms to C_s-m symmetry (Figure 1). This

(25) SHELXTL Plus 4.11, Siemens Analytical X-ray Instruments, Inc., 6300 Enterprise Lane, Madison, WI 53719-1173.

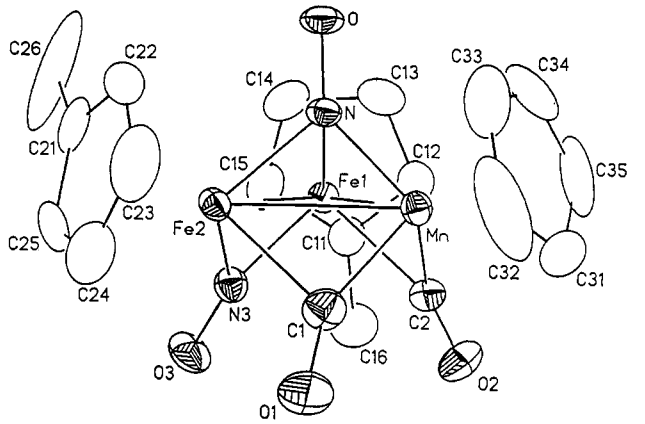

Figure 1. Molecular configuration of the 48-electron $CpMnFe_2Cp'_2(\mu_2\text{-}CO)_2(\mu_2\text{-}NO)(\mu_3\text{-}NO)$ (1). Its $MnFe_2(\mu_2\text{-}CO)_2(\mu_2\text{-}NO)(\mu_3\text{-}NO)$ core has an idealized C_s-m geometry with the pseudomirror plane bisecting the Mn atom, the μ_2-NO ligand, and the μ_3-NO ligand. Atomic thermal ellipsoids are drawn at the 30% probability level.

Table 2. Selected Interatomic Distances (Å) and Bond Angles (deg) for $CpMnFe_2Cp'_2(\mu_2\text{-}CO)_2(\mu_2\text{-}NO)(\mu_3\text{-}NO)$ (1) and $Cp'MnFe_2Cp_2(\mu_2\text{-}CO)_2(\mu\text{-}NO)(\mu_3\text{-}NO)$ (7)[a]

	1	7
Fe1–Fe2	2.452(1)	2.441(2)
Fe1–Mn	2.554(1)	2.555(2)
Fe2–Mn	2.554(1)	2.567(2)
M–M(av)	2.52	2.52
Fe1–(μ_3-NO)	1.895(4)	1.897(2)
Fe2–(μ_3-NO)	1.905(4)	1.902(3)
Mn–(μ_3-NO)	1.890(4)	1.8852)
M–(μ_3-NO)(av)	1.90	1.89
Fe–(μ_2-NO)(av)	1.82	1.81
Fe–(μ_2-CO)(av)	2.12	2.14
Mn–(μ_2-CO)(av)	1.85	1.85
μ_3-(N–O)	2.232(5)	1.254(3)
μ_2-(N–O)	1.214(6)	1.2(3)
μ_2-(C–O)(av)	1.16	1.17
Fe–Cp(av)	2.11	2.11
Mn–Cp(av)	2.11	2.14
Fe1–Mn–Fe2	57.4(1)	56.9(1)
Fe2–Fe1–Mn	61.3(1)	61.8(1)
Mn–Fe2–Fe1	61.3(1)	61.2(1)

[a] Reference 3. [b] M, denotes Fe and/or Mn. [c] Mean M–Cp distances are calculated as an average of the M–C distances from the metal to the ring carbons of the Cp and Cp′ ligands.

core consists of an isosceles triangle of two iron atoms and a manganese atom with each of the two Fe–Mn edges (2.554 Å) spanned by a carbonyl ligand and the Fe–Fe edge (2.452 Å) spanned by a nitrosyl ligand. The $MnFe_2$ triangle is capped with a centered nitrosyl ligand.

The composition of 1 differs from that of the previously published 7[3] by the complete interchange of Cp and Cp′ ligands on the metal atoms (i.e., 1 contains two FeCp′ fragments and one MnCp fragment, while 7 contains two FeCp fragments and one MnCp′ fragment). A comparison of selected interatomic distances and bond angles in 1 and 7 is presented in Table 2; the close similarity of the geometries of these two 48-electron clusters is readily apparent, and the mean metal–metal and metal–ligand distances are virtually identical for 1 and 7.

That the mean M–(μ_3-NO) distances in 1 and 7 are within 0.01 Å of each other would suggest that the Cp′M π symmetry orbitals (SOs) are similar in energy to the CpM π SOs and that their back-bonding interactions with the π^*(NO) orbitals are analogous. However, recent studies[2p] on a series of 48- and 47-electron triangular cobalt clusters, $[Co_3Cp^*_{3-x}Cp'_x(\mu_3\text{-}CO)(\mu_3\text{-}NH)]^n$ (where Cp* denotes η^5-C_5Me_5; x = 0–2; n = 0, 1+), indicated that back-bonding interactions between the π^*(CO) acceptor orbitals and the Cp*Co π donor SOs are significantly stronger than comparable interactions between the π^*(CO) acceptor orbitals and the Cp′CO π donor SOs. This conclusion was based upon the observed shortening of the Cp*Co–CO distance relative to the Cp′Co–CO distance by 0.022 Å in the 48-electron $Cp^*Cp'_2Co_3$ neutral parent and by 0.07 Å in its 47-electron monocation. Thus, we suggest that the equivalent M–(μ_3-NO) distances observed in the $MnFe_2$ cores of 1 and 7 are mainly a consequence of the different electron densities on the metal atoms (arising from the interchange of the Cp and Cp′ ligands) being delocalized over the μ_2-NO and μ_2-CO ligands as well as over the μ_3-NO ligand. If so, the net differences between specific metal–ligand bond lengths would be too small to be detected from our X-ray crystallographic analysis.

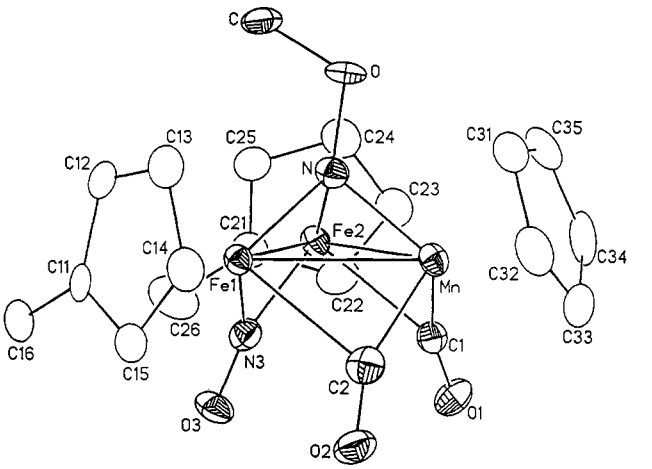

Figure 2. Configuration of the 48-electron $[CpMnFe_2Cp'_2(\mu_2\text{-}CO)_2(\mu_2\text{-}NO)(\mu_3\text{-}NOMe)]^+$ monocation (2) (as the $[CF_3SO_3]^-$ salt). Its $MnFe_2(\mu_2\text{-}CO)_2(\mu_2\text{-}NO)(\mu_3\text{-}NOMe)$ core closely conforms to C_s symmetry. The $(\mu_3\text{-}NOMe)^+$ ligand lying on the pseudomirror plane has a N–O–C bond angle of 114.9(6)°. Atomic thermal ellipsoids are drawn at the 30% probability level. The geometrical features of the related 48-electron $[Cp'MnFe_2Cp_2(\mu_2\text{-}CO)_2(\mu_2\text{-}NO)(\mu_3\text{-}NOMe)]^+$ monocation (3) (as the $[CF_3SO_3]^-$ salt) also closely conform the C_s symmetry, with the μ_3-NOMe ligand lying on the pseudomirror plane displaying a N–O–C bond angle of 115.8(3)°.

Comparison of Structural Features of the $[CpMnFe_2Cp'_2(\mu_2\text{-}CO)_2(\mu_2\text{-}NO)(\mu_3\text{-}NOMe)]^+$ Monocation (2) and the $[Cp'MnFe_2Cp_2(\mu_2\text{-}CO)_2(\mu_2\text{-}NO)(\mu_3\text{-}NOMe)]^+$ Monocation (3). The monoclinic unit cell ($C2/c$) of [2]-$[CF_3SO_3]\cdot{}^1/_2CH_2Cl_2$ contains one crystallographically independent monocation (2) and $[CF_3SO_3]^-$ monoanion occupying the 8-fold general positions, together with an independent CH_2Cl_2 solvent molecule occupying one set of 4-fold crystallographic C_2-2 positions. No unusually short intermolecular contacts indicative of hydrogen-bonding or ion-pairing are observed. The independent 2 is structurally analogous to its precursor (1), but the capping μ_3-NO ligand of the 48-electron neutral parent has been replaced with an electronically equivalent capping $(\mu_3\text{-}NOMe)^+$ ligand. Its $MnFe_2(\mu_2\text{-}CO)_2(\mu_2\text{-}NO)(\mu_3\text{-}NOMe)$ core closely conforms to an idealized C_s-m geometry with the Mn atom, the μ_2-NO ligand, and the $(\mu_3\text{-}NOMe)^+$ ligand passing through the pseudomirror plane within 0.05 Å. Figure 2 shows the geometry and atomic labeling scheme

Table 3. Selected Interatomic Distances (Å) and Bond Angles (deg) for [CpMnFe₂Cp′₂(μ₂-CO)₂(μ₂-NO)(μ₃-NOH)]⁺ (4) ([4][CF₃′SO₃]), [CpMnFe₂Cp′₂(μ₂-CO)₂(μ₂-NO)-(μ₃-NOMe)]⁺ (2) ([2][CF₃SO₃]·½CH₂Cl₂], and [(Cp′MnFe₂Cp₂(μ₂-CO)₂(μ₂-NO)(μ₃-NOMe)]⁺ (3) ([3][CF₃SO₃])

	[4][CF₃SO₃]	[2][CF₃SO₃]	[3][CF₃SO₃]
Fe1–Fe2	2.425(1)	2.457(2)	2.448(1)
Fe1–Mn	2.572(1)	2.590(2)	2.568(1)
Fe2–Mn	2.576(1)	2.580(2)	2.574(1)
M–M(av)[a]	2.52	2.54	2.53
Fe1–(μ₃-NO)	1.854(4)	1.848(7)	1.848(3)
Fe2–(μ₃-NO)	1.840(4)	1.847(7)	1.850(3)
Mn–(μ₃-NO)	1.841(4)	1.870(7)	1.855(4)
M–(μ₃-NO)(av)	1.85	1.86	1.85
Fe–(μ₂-NO)(av)	1.83	1.83	1.81
Fe–(μ₂-CO)(av)	2.18	2.23	2.20
Mn–(μ₂-CO)(av)	1.85	1.85	1.85
μ₃-(N–O)	1.402(5)	1.406(9)	1.406(5)
μ₂-(N–O)	1.205(5)	1.214(10)	1.220(5)
μ₂-(C–O)(av)	1.16	1.16	1.16
Fe–Cp′(av)	2.10	2.11 [Fe-Cp(av)[b]]	2.10
Mn–Cp(av)	2.13	2.13 [Mn-Cp′(av)]	2.15
Fe1–Mn–Fe2	56.2(1)	56.8(1)	56.9(1)
Fe2–Fe1–Mn	62.0(1)	61.4(1)	61.7(1)
Mn–Fe2–Fe1	61.8(1)	61.8(1)	61.4(1)
N–O–R	118 (R = H)	114.9(6) (R = Me)	115.8(3) (R = Me)

[a] M denotes Fe and/or Mn. [b] Mean M–Cp distances are calculated as an average of the M–C distances.

for **2**.

3 differs from **2** only by the interchange of the Cp and Cp′ ligands; it also displays an idealized C_s-*m* geometry with a maximum atomic deviation of only 0.03 Å from the pseudomirror plane. The two crystallographically related cations and anions in the triclinic unit cell ($P\bar{1}$) do not engage in any unusual intermolecular interactions.

As seen from a comparison of selected bond lengths and angles between **2** and **3** in Table 3, the geometries and corresponding interatomic distances of these two monocations are virtually identical within experimental error. As also observed in the comparison between **1** and **7**, the geometrical effects of the Cp′ and Cp ligands on the common core geometry appear to be minimal.

Structural Features of the Monocation [CpMnFe₂Cp′₂(μ₂-CO)₂(μ₂-NO)(μ₃-NOH)]⁺ (4). The orthorhombic unit cell (*Pbcn*) of [4][CF₃SO₃] consists of eight crystallographically related pairs of monocations **4** and [CF₃SO₃]⁻ monoanions which are linked through a NOH···O hydrogen-bonding interaction of 1.7 Å between the hydrogen atom and O(5) of the [CF₃SO₃]⁻ anion. Figure 3 illustrates this cation/anion linkage with a view of **4** and its hydrogen-bonded [CF₃SO₃]⁻ anion. Selected bond lengths and angles for **4** are presented in Table 3.

4 is structurally related to its precursor (**1**) by the formal protonation of the μ₃-NO ligand in the 48-electron neutral parent molecule to give an isoelectronic (μ₃-NOH)⁺ ligand. Its MnFe₂(μ₂-CO)₂(μ₂-NO)(μ₃-NOH) core exhibits the same pseudo-C_s-*m* symmetry as do **1**, **2**, **3**, and **7** with the Mn atom, μ₂-NO ligand, (μ₃-NOH)⁺ ligand, and O(5) of the triflate anion establishing the pseudomirror plane of the core with a maximum atomic deviation of 0.2 Å for the hydrogen atom. The orientation on the (μ₃-NOH)⁺ ligand is virtually identical to that of the corresponding (μ₃-NOMe)⁺ ligand in both **2** and **3**. An examination of Table 3 shows that the corresponding bond lengths are analogous for **2**–**4**. Furthermore, the N–OH bond length of 1.402(5) Å in **4** compares favorably with the N–OH distance of 1.393(4) Å found in the electronically equivalent [Mn₃Cp′₃(μ₂-NO)₃(μ₃-NOH)]⁺ monocation.[11]

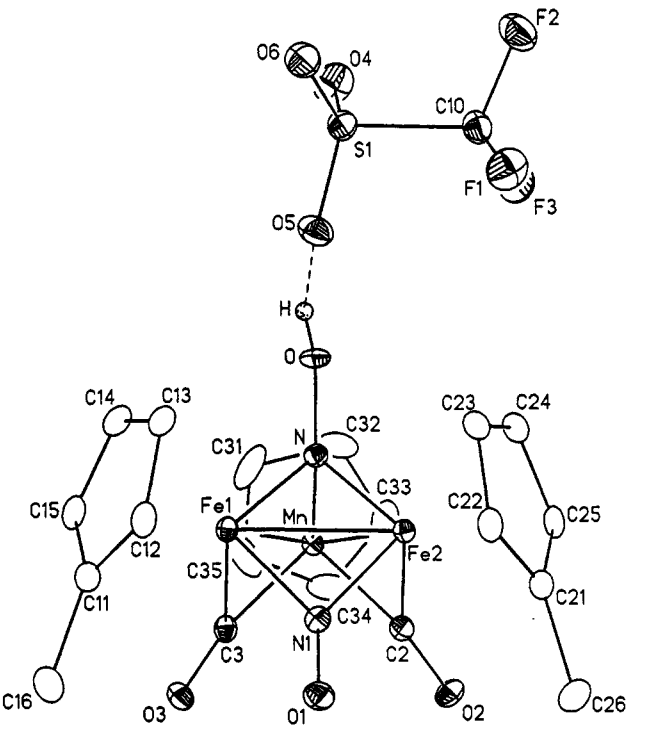

Figure 3. Configuration of the 48-electron [CpMnFe₂Cp′₂(μ₂-CO)₂(μ₂-NO)(μ₃-NOH)]⁺ monocation (**4**) (as the [CF₃SO₃]⁻ salt). The triflate anion is linked to monocation **4** by an O–H···O hydrogen-bonding interaction; the hydrogen atom of the μ₃-NOH ligand located from an electron-density difference map gives rise to a N–O–H bond angle of 118°. Atomic thermal ellipsoids are drawn at the 30% probability level.

Table 4. Selected Interatomic Distances (Å) and Bond Angles (deg) for [Cp′MnFe₂Cp₂(μ₂-CO)₂(μ₂-NO)(μ₃-NH)]⁺ (5) (as [5][PF₆],[a] [5][FeBr₄], and [5][BPh₄]·½THF)

	[5][PF₆]	[5][FeBr₄]	[5][BPh₄]
Fe1–Fe2	2.429(5)	2.426(2)	2.430(2)
Fe1–Mn	2.576(5)	2.593(2)	2.559(2)
Fe2–Mn	2.586(5)	2.585(3)	2.570(2)
M–M(av)[b]	2.53	2.535	2.52
Fe1–(μ₃-NH)	1.87(2)	1.84(1)	1.831(7)
Fe2–(μ₃-NH)	1.94(2)	1.84(1)	1.837(7)
Mn–(μ₃-NH)	1.85(2)	1.86(1)	1.843(6)
M–(μ₃-NH)(av)	1.89	1.85	1.84
Fe–(μ₂-NO)(av)	1.82	1.83	1.83
Fe–(μ₂-CO)(av)	2.18	2.22	2.17
Mn–(μ₂-CO)(av)	1.86	1.85	1.85
μ₂-(N–O)	1.22(3)	1.21(1)	1.20(1)
μ₂-(C–O)(av)	1.16	1.16	1.15
Fe–Cp(av)[c]	2.11	2.09	2.08
Mn–Cp(av)[c]	2.13	2.15	2.11
Fe1–Mn–Fe2	56.1(1)	55.9(1)	56.5(1)
Fe2–Fe1–Mn	62.1(1)	61.9(1)	62.0(1)
Mn–Fe2–Fe1	61.7(1)	62.2(1)	61.5(1)

[a] Reference 24. [b] M denotes Fe and/or Mn. [c] Mean M–Cp distances are calculated as an average of the M–C distances from the metal to the ring carbons of the Cp and Cp′ ligands.

Comparison of Structural Features of the [Cp′MnFe₂Cp₂(μ₂-CO)₂(μ₂-NO)(μ₃-NH)]⁺ Monocation (5) in [5][BPh₄], [5][FeBr₄], and [5][PF₆]. A comparison of corresponding bond lengths and angles for **5** as its [BPh₄]⁻, [FeBr₄]⁻, and [PF₆]⁻ salts is presented in Table 4. The monocation (Figure 4) has the same triangular metal array

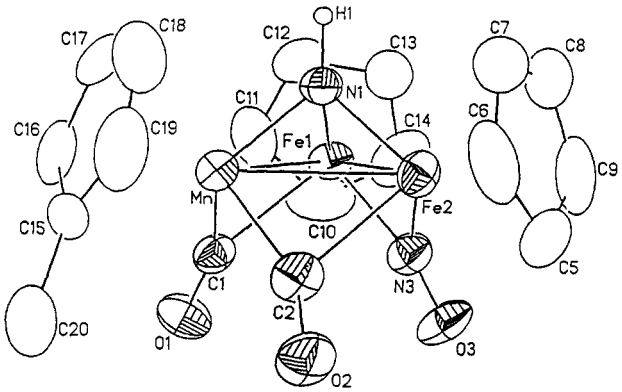

Figure 4. Configuration of the 48-electron $[Cp'MnFe_2Cp_2'(\mu_2\text{-}CO)_2(\mu_2\text{-}NO)(\mu_3\text{-}NH)]^+$ monocation (**5**) (as the $[BPh_4]^-$ salt). Its $MnFe_2(\mu_2\text{-}CO)_2(\mu_2\text{-}NO)(\mu_3\text{-}NH)$ core closely adheres to C_s symmetry with the pseudomirror plane bisecting the Mn atom, the μ_2-NO ligand, and the μ_3-NH ligand. The geometrical features and atomic labeling scheme of monocation **5** as the $[FeBr_4]^-$ salt are similar to those of **5** as the $[BPh_4]^-$ salt. Atomic thermal ellipsoids are drawn at the 30% probability level.

and doubly bridging ligands of pseudo-C_s-*m* symmetry as does its precursor (**7**), but the capping μ_3-NO ligand has been replaced by an electronically equivalent $[\mu_3\text{-}NH]^+$ ligand in **5**. For both **[5][BPh4]** and **[5][FeBr4]**, the hydrogen atom of the μ_3-NH ligand was inserted with idealized coordinates at a distance of 0.96 Å from the nitrogen atom; the positional parameters were tied to those of the coordinated nitrogen atoms. In each compound the isotropic thermal parameter refined to a physically meaningful value comparable to the equivalent isotropic values for the coordinated nitrogen atom.

The monoclinic unit cell ($P2_1/n$) of **[5][BPh4]** contains four crystallographically related pairs of monocations (**5**) and $[BPh_4]^-$ monoanions along with two crystallographically related THF molecules of solvation which are each disordered around a center of symmetry. These cation, anion, and solvent molecules of **[5][BPh4]** have no abnormally short intermolecular contacts, and the $MnFe_2(\mu_2\text{-}CO)_2(\mu_2\text{-}NO)(\mu_3\text{-}NH)$ core (displayed in Figure 5) conforms to an idealized C_s geometry. Due to the number of positional parameters introduced by the $[BPh_4]^-$ anion, the phenyl groups were each constrained to D_{6h} symmetry with a fixed C–C bond distance of 1.39 Å.

The monoclinic unit cell ($P2_1/c$) of **[5][FeBr4]** contains one crystallographically independent monocation (**5**) and $[FeBr_4]^-$ monoanion which are linked by a N–H···Br contact of 2.72 Å. The four Fe–Br distances in the tetrahedral $[FeBr_4]^-$ monoanion vary from 2.289(4) to 2.357(3) Å; the mean distance of 2.34 Å is similar to that of 2.32 Å reported[26] for the two independent $[FeBr_4]^-$ monoanions in $[NMeH_3]_2^+[FeBr_4]^-[Br]^-$. Its formation in **[5][FeBr4]** is presumed to occur via combination of an Fe(III) atom, obtained from the decomposition of another $MnFe_2$ cluster, with four Br^- anions from the Br_2 oxidant.

The relatively large esds associated with the structural parameters of **[5][PF6]** are due to problems encountered in the refinement[24] of this unpublished structure. **[5][PF6]** crystallizes with two independent cations and anions and exhibits significant crystallographic disordering of the $[PF_6]^-$ anions. Each $[PF_6]^-$ anion is linked to the cation by a N–H···F interaction. Aside from the slight triangular

(26) Sproul, G. D.; Stucky, G. D. *Inorg. Chem.* **1972**, *11*, 1647–1650.

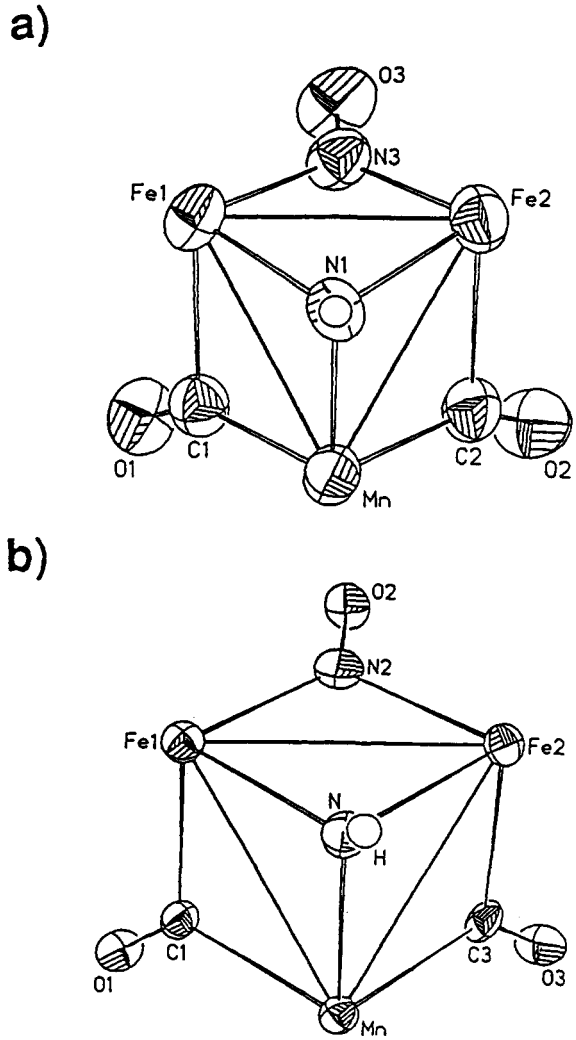

Figure 5. Views of the $MnFe_2(\mu_2\text{-}CO)_2(\mu_2\text{-}NO)(\mu_3\text{-}NH)$ core in (a) the 48-electron monocation **5** (from $[5]^+[BPh_4]^-$) with pseudo-C_s symmetry and (b) the neutral 49-electron **6** with pseudo-C_{3v} symmetry. Upon a one-electron reduction of the core, only the Fe–Fe bond is presumed (from related work) to lengthen markedly relative to the two Fe–Mn bonds, resulting in a nearly equilateral metal triangle. Unfortunately, a crystal disordering of **6** precludes a more definitive comparison of core geometries.

metal variations attributed to differing packing forces, the close cation/anion intermolecular contacts found in the $[PF_6]^-$ and $[FeBr_4]^-$ salts of **5** do not appear to significantly affect the common $MnFe_2(\mu_2\text{-}CO)_2(\mu_2\text{-}NO)(\mu_3\text{-}NH)$ core geometry; the core bond lengths and angles in these salts are similar to those found in **[5][BPh4]** which has no short intermolecular cation/anion contacts.

Crystal and Structural Features of $Cp'MnFe_2Cp'_2(\mu_2\text{-}CO)_2(\mu_2\text{-}NO)(\mu_3\text{-}NH)$ (6). The triclinic unit cell ($P\bar{1}$) of **6** consists of two crystallographically related discrete molecules which pack with no unusually short intermolecular contacts. The $MnFe_2$ core of **6** was modeled as a single orientation, but the analogous coordination of a Cp′ ligand to each metal atom and the observed pseudo-C_{3v} symmetry make it highly probable that the observed molecular architecture corresponds to an "averaged structure" due to 3-fold rotational disorder of the three MCp′ fragments and their one doubly bridging nitrosyl and two doubly bridging carbonyl ligands. The three M–M distances of 2.563(2), 2.579(2), and 2.586(2) Å are approximately equivalent, and the μ_3-NH ligand is centered

over the pseudoequilateral triangle (M–N, 1.863(7), 1.865(7), and 1.870(6) Å). The three pseudomirror planes each bisect a metal atom, a doubly bridging ligand, and the μ_3-NH ligand. A view of the core of **6** is presented in Figure 5.

Discussion

Structural-Bonding Comparison of the 48-Electron Clusters $CpMnFe_2Cp'_2(\mu_2\text{-}CO)_2(\mu_2\text{-}NO)(\mu_3\text{-}NO)$ (1), $[Cp'MnFe_2Cp_2(\mu_2\text{-}CO)_2(\mu_2\text{-}NO)(\mu_3\text{-}NOMe)]^+$ (3), $[CpMnFe_2Cp'_2(\mu_2\text{-}CO)_2(\mu_2\text{-}NO)(\mu_3\text{-}NOH)]^+$ (4), and $[Cp'MnFe_2Cp_2(\mu_2\text{-}CO)_2(\mu_2\text{-}NO)(\mu_3\text{-}NH)]^+$ (5). Tables 2–4 present the relevant interatomic distances and bond angles used in the bonding analysis below.

One of the most striking structural features of these 48-electron neutral and cationic triangular metal clusters is the insensitivity of the metal–metal bonding interactions to changes in cluster charge and to changes in the composition and bonding characteristics of the nitrogen-containing capping ligand. The cores of **1–5** and **7** all exhibit a pseudomirror plane symmetry with very similar Fe–Fe (2.44 ± 0.01 Å) and mean Fe–Mn (2.57 ± 0.01 Å) distances.

A substantial change is observed in both the capping Fe–N and Mn–N distances upon transformation of the μ_3-NO ligands of **1** and **7** into the $(\mu_3\text{-}NX)^+$ ligands (where X = OMe for **3**, OH for **4**, and H for **5**). The average M–N distance decreases from 1.89–1.90 Å in **7** and **1** to 1.84–1.85 Å in the monocation complexes, presumably due to enhanced electron-accepting capacities of the $(\mu_3\text{-}NOR)^+$ (R = Me, H) and $(\mu_3\text{-}NH)^+$ ligands relative to that of the μ_3-NO ligand.

The NO ligand may be viewed as being composed of sp-hybridized N and O atoms which interact to form two orthogonal π/π^* combinations. For the M–(μ_3-NO) bonding in **1**, one of these empty π^* nitrosyl orbitals may be considered to be parallel with the Fe–Fe bond, while the other π^* nitrosyl orbital is directed toward the Mn atom. Strong $3d\pi$ metal→π^*(NO) back-bonding interactions would decrease the M–N distances and increase the N–O distance. Upon the addition of either a Me^+ adduct or an H^+ adduct to the μ_3-NO ligand to form a $(\mu_3\text{-}NOR)^+$ ligand (R = Me, H), the oxygen atom is assumed to become sp^2-hybridized, leaving only one p oxygen AO available for π bonding to the sp-hybridized nitrogen atom; thus the nitrogen atom has its remaining unhybridized p AO available for exclusive metal–nitrogen bonding. The sizable lengthening in the trimetal-capped N–O distance from 1.24–1.25 Å in **1** and **7** to values of 1.40–1.41 Å in **2–4** is consistent with a marked weakening of the N–O bond in the $(\mu_3\text{-}NOR)^+$ ligands (R = Me, H). The experimentally determined N–O–R bond angles of 114.9(6)° in **2**, 115.8(3)° in **3**, and 118° in **4** support this conceptualized bonding view that the oxygen atom has sp^2 hybridization. The hybridized orbitals lie in the pseudomirror plane perpendicular to the Fe–Fe bond. Thus, the one remaining π^*(NO) orbital in **2–4** is parallel with the Fe–Fe bond, indicating that $d\pi$(Fe)→π^*(NO) back-bonding interactions are considerably greater than the corresponding $d\pi$(Mn)→π^*(NO) interaction. The superior π^*(NO) acceptor ability of the electron-deficient $(\mu_3\text{-}NOR)^+$ ligand in **2–4** relative to the (μ_3-NO) ligand in **1** and **7** is reflected by significantly shorter Fe–N distances to the trimetal capping ligands. The decreased Mn–N distances in **2–4** relative to those in **1** and **7** are attributed to enhanced metal–ligand π-bonding via the p(N) AO in the $(\mu_3\text{-}NOR)^+$ ligand which is directed toward the Mn atom. The much greater electron-accepting capacities of the $(\mu_3\text{-}NOR)^+$ ligands must be a consequence of positive-charge polarization effects, such that these ligands withdraw more electron density from the common $MnFe_2(\mu_2\text{-}CO)_2(\mu_2\text{-}NO)$ fragment than does the neutral μ_3-NO ligand. An increase in the mean Fe–(μ_2-CO) distances (viz., 2.12 Å in **1** vs 2.20 Å in **3** and 2.18 Å in **4**) and a higher frequency shift of ca. 30–40 cm^{-1} of the μ_2-CO infrared absorption bands indicate that the $d\pi$(Fe)→π^*(CO) back-bonding interactions have markedly decreased in **3** and **4** due to the enhanced $d\pi$(Fe)→π^*(NOR) back-bonding interactions. These crystallographic/spectral data are thereby consistent with a redistribution of electron density away from the common $MnFe_2(\mu_2\text{-}CO)_2(\mu_2\text{-}NO)$ fragment to the more positively-charged $(\mu_3\text{-}NOR)^+$ ligand in **2–4**.

The electron-deficient $(\mu_3\text{-}NH)^+$ ligand in **5** exhibits metal-to-bridging ligand distances which are similar to those found in **2–4**. The relatively short Mn–(μ_3-NH) and Fe–(μ_3-NH) distances observed in **5** are likewise attributed to enhanced π bonding of the two p(N) AOs with corresponding $d\pi$(Mn) and $d\pi$(Fe) orbitals due to the electron-deficient nature of the three-electron donating $(\mu_3\text{-}NH)^+$ ligand relative to that of the three-electron donating neutral (μ_3-NO) ligand in **1** and **7**.

Structural-Bonding Comparison of the 48/49-Electron $[(\eta^5\text{-}C_5H_4Me)MnFe_2(\eta^5\text{-}C_5H_{5-x}Me_x)_2(\mu_2\text{-}CO)_2(\mu_2\text{-}NO)(\mu_3\text{-}NH)]^n$ Series (Where $x = 0$, $n = 1+$ for 5; $x = 1$, $n = 0$ for 6). Table 5 and Figure 5 summarize the geometrical changes which occur upon reduction of a 48-electron $MnFe_2$ cluster with a capping μ_3-NH ligand to a 49-electron system. This one-electron reduction of an imido-capped monocation (**5**) to its neutral analogue (**6**) gives rise to a significant change in the overall geometry of the $MnFe_2(\mu_2\text{-}CO)_2(\mu_2\text{-}NO)(\mu_3\text{-}NH)$ core from an idealized C_s configuration in the 48-electron system to a pseudo-C_{3v} geometry in the 49-electron complex (**6**).

In the analogous 48/49-electron $[Cp'MnFe_2Cp_2(\mu_2\text{-}CO)_2(\mu_2\text{-}NO)(\mu_3\text{-}NO)]^n$ series (where $n = 0$ for **7**; $n = -1$ for $\mathbf{7}^-$) synthesized and examined by Kubat-Martin *et al.*,[3] the C_s idealized crystal-ordered geometry of **7** was maintained

Table 5. Selected Interatomic Distances (Å)[a] and Bond Angles (deg) for $[Cp'MnFe_2Cp_2(\mu_2\text{-}CO)_2(\mu_2\text{-}NO)(\mu_3\text{-}NH)]^+$ (5) ([5][BPh_4]) and $Cp'MnFe_2Cp'_2(\mu_2\text{-}CO)_2(\mu_2\text{-}NO)(\mu_3\text{-}NH)$ (6)[b]

	5	6	Δ (Å)
Fe1–Fe2	2.43	2.58	0.15
Fe–Mn(av)	2.57	2.57	0.00
M–M(av)[c]	2.52	2.58	+0.06
Fe1–(μ_3-NH)(av)	1.83	1.86	0.03
Mn–(μ_3-NH)	1.84	1.87	0.03
M–(μ_3-NH)(av)	1.84	1.87	+0.03
Fe–(μ_2-NO)(av)	1.83	1.87	
Fe–(μ_2-CO)(av)	2.17	1.91	
Mn–(μ_2-CO)av	1.85	1.95	
M–(μ_2-XO)[d]	1.95	1.91	–0.04
Fe1–Mn–Fe2	56.5	60.1	
Fe2–Fe1–Mn	62.0	60.4	
Mn–Fe2–Fe1	61.5	59.5	

[a] Interatomic distances are rounded off to the hundredth of an Å. [b] The M–M and M–ligand distances given are for the single major orientation modeled in the crystal-disordered system. [c] M denotes Fe and/or Mn. [d] X denotes either N or C. Specific M–(μ_2-XO) distances cannot be unambiguously determined in the crystal-disordered molecule **6**.

upon reduction to 7^- with an observed elongation of 0.16 Å in only the Fe–Fe bond length. This significant increase of the Fe–Fe bond length with essentially no changes in the two Mn–Fe bond lengths was rationalized via a bonding analysis involving localization of the added unpaired electron in an antibonding orbital combination between the two Fe atoms such that the half-filled nondegenerate HOMO (of a″ representation under C_s symmetry) is antisymmetric with respect to the mirror plane.[3] Definitive support for this bonding analysis was provided by an EPR solution spectrum which displayed a single narrow line (g = 1.97; 25-G line width at 22 °C) with no evidence of any hyperfine structure, thus indicating that the unpaired electron occupies a HOMO with no detectable ^{55}Mn (I = $^5/_2$) or ^{14}N (I = 1) orbital character.

Although the apparent 3-fold crystal disorder found in the 49-electron **6** precludes rigorous comparison of the changes in specific bond lengths and angles, the mean M–M bond distance increase of 0.06 Å observed upon the one-electron reduction of the 48-electron (μ_3-NH)-containing monocation to its 49-electron neutral analogue compares favorably to the observed increase of 0.05 Å in the mean M–M distance upon the similar reduction of the (μ_3-NO)-containing **7** to its monoanion.[3] The room-temperature EPR solution spectrum of **6** is analogous to that observed for 7^-, displaying a single line (g = 2.033; 37-G line width at 27 °C) with no discernible hyperfine structure. Thus, the added unpaired electron in the imido-capped **6** is associated primarily with the two iron atoms, as was determined for the nitrosyl-capped 7^-.

The observed increase of 0.03 Å in the mean M–(μ_3-NH) distances and decrease of 0.04 Å in the mean M–(μ_2-XO) distances (X = C or N) in the crystal-disordered 49-electron **6** relative to the crystal-ordered 48-electron monocation **5** are similar to the mean bond-length variations observed upon reduction of **7** to 7^-. A commensurate lower frequency shift of 10–20 cm^{-1} in the infrared absorption bands is observed for the doubly bridging CO and NO ligands upon reduction of each system, reflecting the redistribution of electron density away from the tricapping ligand.

Synthesis of $[Cp'MnFe_2Cp_2(\mu_2\text{-}CO)_2(\mu_2\text{-}NO)(\mu_3\text{-}NH)]^+$ (5) from $Cp'MnFe_2Cp_2(\mu_2\text{-}CO)_2(\mu_2\text{-}NO)(\mu_3\text{-}NO)$ (7). Kubat-Martin *et al.*[3,24] first synthesized the imido-capped monocation (**5**) in an attempted oxidation reaction of **7** with $AgPF_6$ to obtain the 47-electron $[Cp'MnFe_2Cp_2(\mu_2\text{-}CO)_2(\mu_2\text{-}NO)(\mu_3\text{-}NO)]^+$ monocation (7^+). **5** is electronically equivalent with and structurally analogous to the imido-capped $[Mn_3Cp'_3(\mu_2\text{-}NO)_3(\mu_3\text{-}NH)]^+$ monocation previously isolated by Legzdins and co-workers.[11] This complex was derived from a ligand-transformation reaction in which a nitrosyl ligand capping a trimetal-bonding $Mn_3Cp'_3(\mu_2\text{-}NO)_3$ fragment was reversibly converted to a $[\mu_3\text{-}NOH]^+$ ligand by the addition of 1 equiv of strong acid, HPF_6(aq), and then irreversibly converted to a $[\mu_3\text{-}NH]^+$ ligand by the addition of another 2 equiv of acid (along with two electrons provided intermolecularly). Kubat-Martin *et al.*,[3,24] proposed that the ligand conversion of the μ_3-NO ligand in **7** to $(\mu_3\text{-}NH)^+$ in **5** involved an electrophilic attack by Ag^+ on the μ_3-NO ligand to give an analogous $[\mu_3\text{-}NOAg]^+$-containing species which could then form the $(\mu_3\text{-}NH)^+$-containing cluster by reaction with a proton source (adventitious water) and an external two-electron source.

However, as reported herein, **5** has been isolated from reactions of **7** with a wide variety of oxidants including $NOBF_4$, NO_2PF_6, Br_2, and I_2. Thus, the transformation of the μ_3-NO ligand in **7** into the $(\mu_3\text{-}NH)^+$ ligand in **5** in these oxidation-induced reductive deoxygenation reactions appears to occur via a different reaction pathway than that determined by Legzdins *et al.*,[11] for the sequential conversion in the trimanganese series of the μ_3-NO ligand to $(\mu_3\text{-}NOH)^+$ and then to the $(\mu_3\text{-}NH)^+$ ligand by protic acids. The oxidants Br_2 and I_2, and to a lesser extent NO^+ and NO_2^+, are not strong Lewis acids like H^+ and Ag^+. Therefore, initial Lewis-acid coordination to the nucleophilic μ_3-NO oxygen atom is not necessarily an essential step in the overall reaction.

The corresponding protonated $[Cp'MnFe_2Cp_2(\mu_2\text{-}CO)_2(\mu_2\text{-}NO)(\mu_3\text{-}NOH)]^+$ monocation has not been isolated from normal protonation reactions of **7**. Reactions of **7** in CH_2Cl_2 with HPF_6(aq) resulted in the formation of an intractable residue, while reactions with less than 0.5 equiv of $HBF_4{\cdot}OMe_2$ produced only the $(\mu_3\text{-}NH)^+$-containing **5**. The yields of **5** obtained from reactions of **7** with $HBF_4{\cdot}OMe_2$ were maximized by the addition of approximately 1.5 equiv of acid instead of the 3 equiv reported[11] for the trimanganese series. In fact, the addition of 3 equiv of $HBF_4{\cdot}OMe_2$ to solutions of **7** resulted in almost complete decomposition of the compound to an uncharacterized insoluble residue. Thus, if a $(\mu_3\text{-}NOH)^+$-containing species *is* formed as an intermediate, its conversion to the $(\mu_3\text{-}NH)^+$-containing cluster must be much more facile for the $MnFe_2$ clusters than for the analogous isolated $(\mu_3\text{-}NOH)^+$-containing trimanganese cluster. The serendipitous isolation of the $(\mu_3\text{-}NOH)^+$-containing **4** from the reaction of **1** with dilute triflic acid (generated via hydrolysis of methyl triflate with adventitious water in the CH_2Cl_2 solvent) indicates that this acid may behave as a more innocent proton source for these mixed-metal clusters.

The isolation of the imido-containing **5** with the $[FeBr_4]^-$ counterion provides substantiation that the origin of the two electrons needed in the formal reduction of each capping μ_3-NO ligand to a $(\mu_3\text{-}NH)^+$ ligand is another $MnFe_2$ cluster, which is the only source of iron in its reaction with Br_2. Reaction of **7** with the milder oxidant I_2 similarly resulted in the isolation of the imido cation (**5**) with a corresponding $[FeI_4]^-$ anion (as determined from an X-ray crystallographic analysis).

Although **7** and the analogous **1** exhibit electrochemically reversible oxidations, all attempts to chemically oxidize these nitrosyl-capped clusters have produced the imido-capped cations along with insoluble residues. One can hypothesize that the N–O bond of the (μ_3-NO) ligand in **1** and **7** is sufficiently weakened in the oxidized species that it may undergo reductive cleavage with a CO or NO ligand of another cluster to form CO_2 or NO_2. The resultant μ_3-N nitrido ligand would then extract a proton from adventitious water to give the $(\mu_3\text{-}NH)^+$ ligand. It is noteworthy that this reaction pathway is related to the reductive deoxygenation of an amine oxide by a carbonyl ligand which results in decarbonylation from a metal carbonyl complex as CO_2.

Attempted N–H and N–O Cleavage Reactions. One primary synthetic goal of deprotonation of the $(\mu_3\text{-}NH)^+$ ligand in **5** and of N–O bond cleavage of the μ_3-NO ligand in **1** and **7** was to isolate and characterize a triangular metal cluster with a "bare" pyramidally-coordinated nitrido ligand. To our knowledge, only one triangular metal complex with such a μ_3-N ligand has been previously

reported.[27,28] A pyramidal nitrogen ligand has been proposed as an intermediate in the interconversion of the wingtip and hinge metal positions in the butterfly-shaped $[FeRu_3N(CO)_{12}]^-$ monoanion.[29] Additionally, *in situ* experiments on the electrochemically-produced $[Co_3Cp_3(\mu_3\text{-}CO)(\mu_3\text{-}NH)]^{2+}$ dication provided evidence for deprotonation with NEt_3 to give a pyramidal nitride cluster.[2j]

The very low-field chemical shift value of 24.9 ppm for the apical proton in the imido-capped **5** suggests that it is fairly acidic and should be easily cleaved from the nitrogen atom. However, this system could not be deprotonated with the weak base NEt_3. Reactions of **5** with Proton Sponge and CH_3Li potentially produced the nitrido complex, but the reaction product isolated by crystallization was the nitrosyl-containing complex **7**.

Acknowledgment. This research was generously supported by the National Science Foundation. We are grateful to a former co-worker Dr. Kimberly Ann Kubat-Martin (now at Los Alamos National Laboratory) for her assistance in the initial phases of this work. Special thanks are extended to Professor Brock Spencer (Beloit College) for his assistance in performing the EPR measurements and to EXTREL FTMS, Millipore Corp. (6416 Schroeder Rd., Madison, WI 53711) for the use of their EXTREL FTMS-2000 spectrometer and for their interest in this project. A.B. gratefully acknowledges the Icelandic Science Foundation, the University of Iceland Research Fund, and the Fulbright Foundation for travel funds which made the mass spectral measurements possible.

Supplementary Material Available: Tables of atomic positions, anisotropic thermal displacement coefficients, interatomic distances, and bond angles for the non-hydrogen atoms and idealized positional and isotropic thermal parameters for the hydrogen atoms of $CpMnFe_2Cp'_2(\mu_2\text{-}CO)_2(\mu_2\text{-}NO)(\mu_3\text{-}NO)$ **(1)**, $[CpMnFe_2Cp'_2(\mu_2\text{-}CO)_2(\mu_2\text{-}NO)(\mu_3\text{-}NOMe)]^+$ **(2)** as the $[CF_3SO_3]^-$ salt, $[Cp'MnFe_2Cp_2(\mu_2\text{-}CO)_2(\mu_2\text{-}NO)(\mu_3\text{-}NOMe)]^+$ **(3)** as the $[CF_3SO_3]^-$ salt, $[CpMnFe_2Cp'_2(\mu_2\text{-}CO)_2(\mu_2\text{-}NO)(\mu_3\text{-}NOH)]^+$ **(4)** as the $[CF_3SO_3]^-$ salt, $[Cp'MnFe_2Cp_2(\mu_2\text{-}CO)_2(\mu_2\text{-}NO)(\mu_3\text{-}NH)]^+$ **(5)** as the $[BPh_4]^-$ and $[FeBr_4]^-$ salts, and $Cp'MnFe_2Cp'_2(\mu_2\text{-}CO)_2(\mu_2\text{-}NO)(\mu_3\text{-}NH)$ **(6)** (30 pages). Ordering information is given on any current masthead page.

OM9300336

(27) The synthesis and structure of a nitrido-capped triangular titanium complex, $Ti_3Cp^*_3(\mu_2\text{-}NH)_3(\mu_3\text{-}N)$, was recently reported by Roesky et al.[28] Its molecular configuration of pseudo C_{3v} symmetry possesses a six-membered chairlike $(TiNH)_3$ ring with the three nonbonding titanium(IV) atoms linked by doubly bridging imido ligands and the triply bridging nitride atom. To our knowledge, this is the only structurally known compound containing a pyramidal μ_3-N ligand.

(28) Roesky, H. W.; Bai, Y.; Noltenmeyer, M. *Angew. Chem., Int. Ed. Engl.* **1989**, *28*, 754–755.

(29) Fjare, D. E.; Gladfelter, W. L. *J. Am. Chem. Soc.* **1984**, *106*, 4799–4810.